Title
Deformation Behavior of Bimodal Nanostructured 5083 Al Alloys

Journal
Metallurgical and Materials Transactions A, 36A

Author
Han, B Q

Publication Date
2005

Peer reviewed

Deformation Behavior of Bimodal Nanostructured 5083 Al Alloys

B.Q. HAN, Z. LEE, D. WITKIN, S. NUTT, and E.J. LAVERNIA

Cryomilled 5083 Al alloys blended with volume fractions of 15, 30, and 50 pct unmilled 5083 Al were produced by consolidation of a mixture of cryomilled 5083 Al and unmilled 5083 Al powders. A bimodal grain size was achieved in the as-extruded alloys in which nanostructured regions had a grain size of 200 nm and coarse-grained regions had a grain size of 1 μm. Compression loading in the longitudinal direction resulted in elastic-perfectly plastic deformation behavior. An enhanced tensile elongation associated with the occurrence of a Lüders band was observed in the bimodal alloys. As the volume fraction of coarse grains was increased, tensile ductility increased and strength decreased. Enhanced tensile ductility was attributed to the occurrence of crack bridging as well as delamination between nanostructured and coarse-grained regions during plastic deformation.

I. INTRODUCTION

LARGE increases in strength are commonly observed in nanostructured metals, a phenomenon that is explained in part by grain refinement and the well-known Hall–Petch relation. However, low ductility, and the associated loss of toughness, is a serious deficiency in most of these metals.[1] High ductility in nanostructured materials has been observed in a few cases, but these cases appear to be exceptional,[2,3] often occurring only at high temperatures[4] or with microtensile samples using specialized testing equipment.[5]

Inspection of the relevant literature reveals that several approaches have been proposed to enhance the ductility of nanostructured materials.[6,7] In one recent study, high tensile ductility was observed in nanostructured Cu with a bimodal grain structure that was achieved by partial annealing.[6] In earlier studies, Tellkamp and co-workers reported on the mechanical properties of a nanostructured cryomilled 5083 Al alloy, with a yield strength of 334 MPa, ultimate strength of 462 MPa, and an elongation of 8.4 pct.[8] They suggested that the presence of coarse grains in the nanocrystalline matrix was responsible for the observed ductility, an observation that sparked the genesis of multiscale materials. In this particular case, the coarse grains arose as a result of thermomechanical processing of the nanostructured powders, *i.e.*, consolidation and extrusion. Multiscale structures were recently produced in a cryomilled Al-Ti-Cu alloy.[9] The microstructure consisted of nanocrystalline grains and elongated coarse-grained bands. Under tensile loading, microcracks nucleated in nanocrystalline regions and propagated to ductile coarse-grained regions, where they were effectively arrested by a combination of crack blunting and crack bridging.

Among the various approaches that are currently being investigated to generate nanostructured materials, cryomilling affords unusual flexibility in microstructural design and the ability to produce bulk samples.[8] As with other methods for producing nanostructured alloys, decreasing grain size is accompanied by decreases in ductility.[10] However, recent reports demonstrate that cryomilled aluminum alloys with an ultrafine-grained microstructure[11] or with a bimodal grain size distribution[8] can attain elongations of 7 to 8 pct, rendering them attractive for many engineering applications.

The present investigation was motivated by the hypothesis that the ductility of nanocrystalline Al alloys can be enhanced by incorporating a more ductile, coarse-grained component. If a small proportion of coarse grains are added to a nanostructured matrix, the material's ductility should increase with only a small decrement in strength. To test this hypothesis, and to elucidate underlying mechanisms, several cryomilled 5083 Al alloys with different volume fractions of unmilled coarse-grained 5083 Al were produced. The same procedures were used that have been employed previously to make fully cryomilled Al alloys.[8,11,12] The microstructural characteristics, mechanical behavior, and deformation mechanisms of these materials were explored in the present study.

II. MATERIALS AND EXPERIMENTAL PROCEDURES

Three bulk alloys of cryomilled 5083 Al (Al-4.2 wt pct Mg-0.67 wt pct Mn), blended with 15, 30, and 50 pct unmilled powders, were produced following procedures similar to those used previously.[8,11,12] Spray-atomized 5083 Al alloy powders were mechanically milled in a liquid nitrogen slurry. The cryomilled powders were blended mechanically with different volume fractions of unmilled 5083 powders (15, 30, and 50 pct, respectively) in an inert atmosphere to achieve a uniform distribution of unmilled powders. The powders used for cryomilling and for the unmilled additions were from the same spray-atomized batch. The various blends of powders were then canned, also under an inert atmosphere. Consolidation of the canned powders was completed by cold isostatic pressing at a pressure of ~400 MPa. The consolidated compacts were vacuum degassed at a temperature of 673 K. To remove any remaining porosity and improve mechanical properties, the consolidated billets were extruded

B.Q. HAN, Assistant Researcher, and E.J. LAVERNIA, Professor, are with the Department of Chemical Engineering and Materials Science, University of California, Davis, CA 95616. Contact e-mail: bqhan@ucdavis.edu Z. LEE, Postdoctoral Researcher, and S. NUTT, Professor, are with the Department of Materials Science, University of Southern California, Los Angeles, CA 90089. D. WITKIN, Research Assistant, is with the Department of Chemical Engineering and Materials Science, University of California, Irvine, CA 92697.

Manuscript submitted September 27, 2004.

into a round bar with a diameter of 19.05 mm at a temperature of 823 K. Some of the extruded 5083 Al alloys were further swaged at a temperature of 723 K. The swaged 5083 Al alloys had a final diameter of 12.7 mm.

Thin foils for transmission electron microscopy (TEM) were sectioned with a diamond saw and laminated with a silicon wafer. The sandwich assemblies were polished mechanically to create a wedge using diamond lapping films of 30 to 0.5 μm and a cloth with colloidal silica. The samples were briefly milled in a low-angle ion mill using a cold stage holder. Samples thus prepared provided large thin areas for TEM observation.

Mechanical performance was evaluated by both tensile and compression tests. The as-extruded materials were machined into flat dog-bone tensile specimens along the extrusion direction, with the gage length of 12 mm, width of 4 mm, and thickness of 2 mm. The gage sections of the tensile specimens were polished close to a mirror finish in order to reduce the effect of surface defects and detect visually possible shear banding. Compression specimens were machined along the extrusion direction, with a cubic configuration measuring 5 mm per edge.

Tensile and compression testing was performed using a universal testing machine (Instron 8801, Canton, MA). The operation of the testing machine was computer-controlled and the digital data of load and displacement from the gage section were recorded. Tensile specimens were tested at a constant crosshead velocity of 0.012 mm/s until failure, with direct measurement of the displacement of the tensile gage section by a dual-camera video extensometer. Compression tests were conducted at a constant crosshead velocity of 0.005 mm/s, with measurement of the displacement of compression platens (including the displacement of specimens and the elastic deformation of platens) by the video extensometer. The elastic deformation of the compression platens, without a sample, was measured after the tests and subtracted from all compression stress-strain curves. The fracture surface of the tensile specimens was studied using a scanning electron microscope (SEM) operated at 10 kV.

Tensile tests of the as-swaged materials were conducted using dog-bone tensile specimens with a gage length of 19 mm and a diameter of 4.6 mm, in a load frame at a constant crosshead velocity of an initial strain rate of 0.016 mm/s.

III. RESULTS

A. *Microstructure*

The microstructure of as-extruded cryomilled 5083 Al alloys is shown in Figure 1, a section taken transverse to the extrusion direction. Equiaxed grains are distributed uniformly in the nanostructured regions of the as-extruded alloy with 30 pct of unmilled powder (Figure 1(a)). The continuous rings in selected area electron diffraction patterns (Figure 1(b)) indicate large misorientations between grains. When viewed normal to the extrusion direction of the sample containing 50 pct unmilled powder (longitudinal sections in Figures 1(c) and (d)), coarse-grained bands from the unmilled powder additions extend in the extrusion direction. Histograms of the grain size distributions in the as-extruded alloys are shown in Figures 1(e) through (h). The mean grain sizes measured from approximately 200 grains are 207 nm for 0 pct, 227 nm for 15 pct, 317 nm for 30 pct, and 629 nm for 50 pct. The number of coarse grains with a grain size of approximately 1000 nm increases with increasing volume fraction of unmilled powder. In addition, the unmilled coarse-grained regions extend in the extrusion direction. The regions are discretely distributed at 15 pct volume fraction, but tend to be more interconnected at 50 pct volume fraction.

B. *Compression Test*

Figure 2(a) shows the compressive true stress *vs* true strain for the as-extruded alloys with 0, 15, 30, and 50 pct unmilled

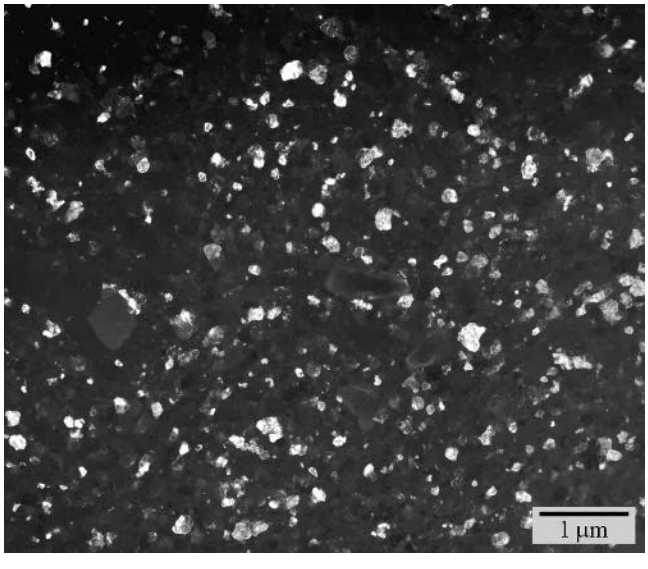

(*a*)

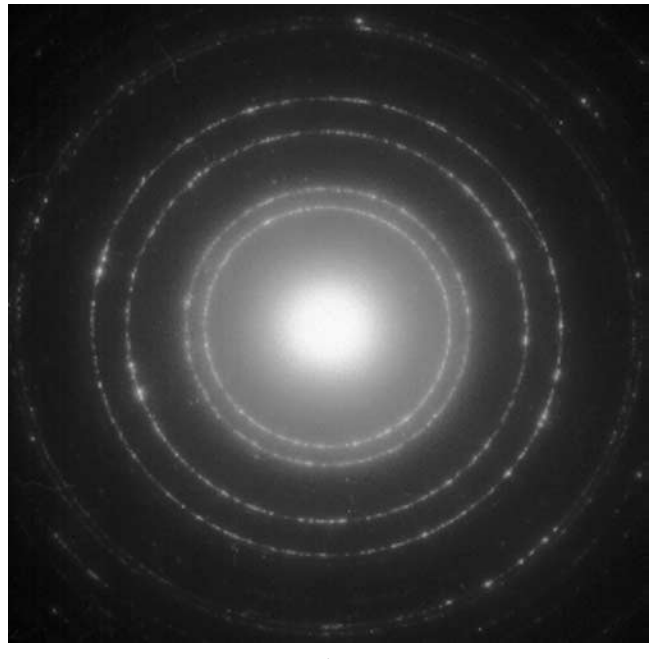

(*b*)

Fig. 1—TEM microstructure of the as-extruded 5083 Al alloys (*a*) and (*b*) with 30 pct of unmilled 5083 Al in a transverse section and (*c*) and (*d*) with 50 pct of unmilled 5083 Al in a longitudinal section; (*e*) to (*h*) histograms of grain sizes of the as-extruded 5083 Al alloys.

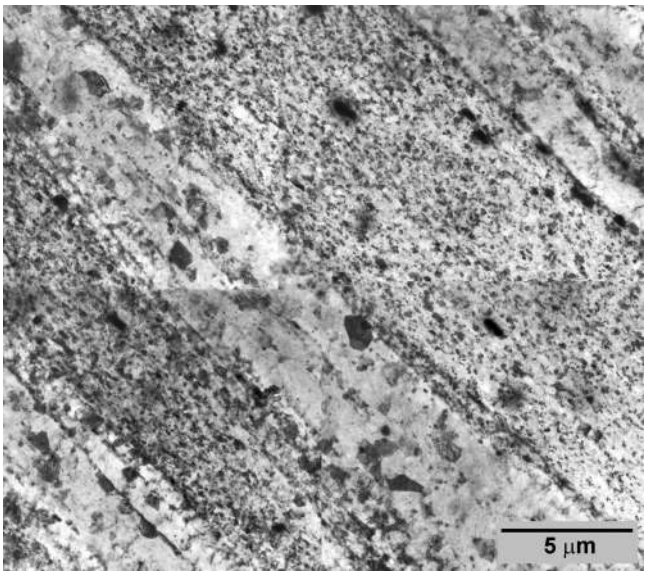

(*c*)

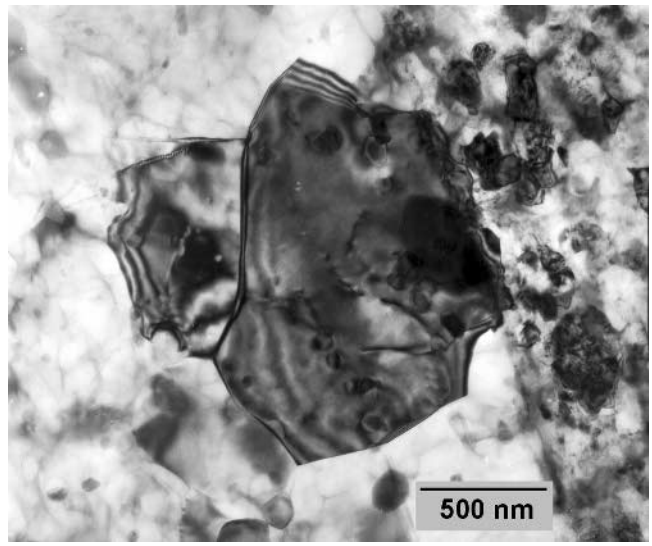

(*d*)

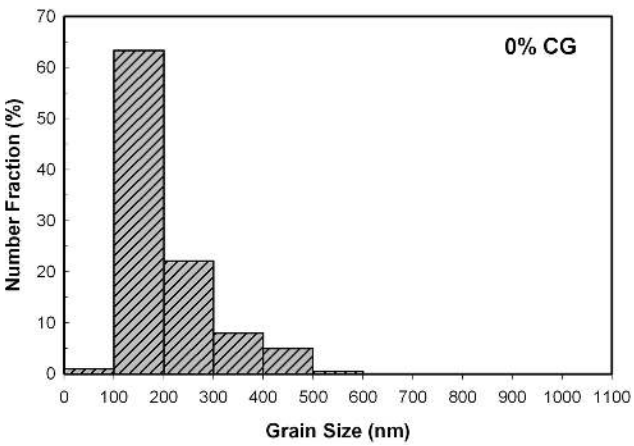

(*e*)

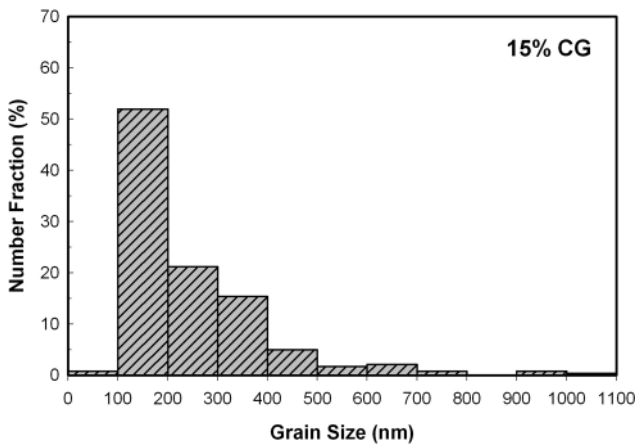

(*f*)

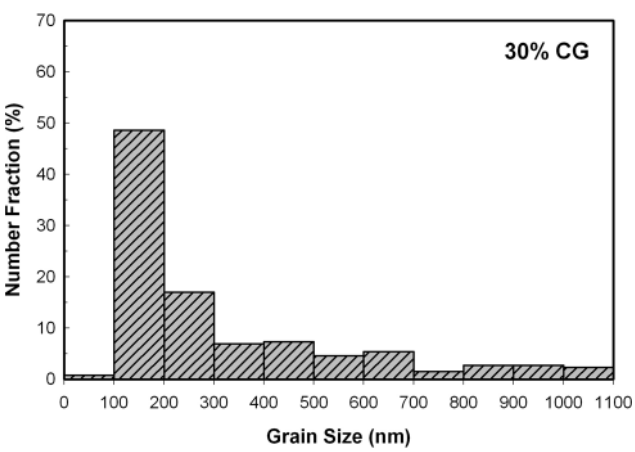

(*g*)

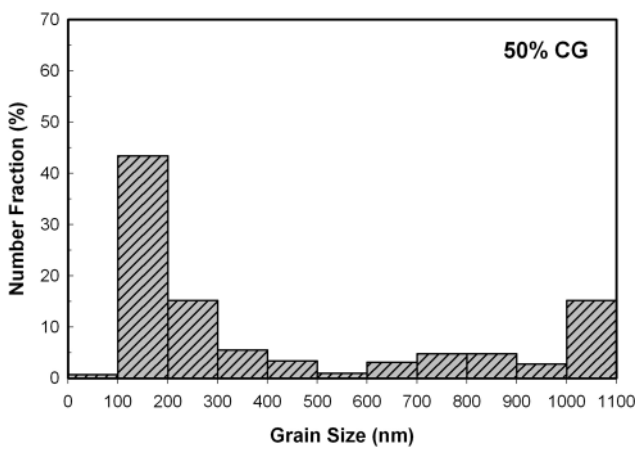

(*h*)

Fig. 1—(Continued). TEM microstructure of the as-extruded 5083 Al alloys (*a*) and (*b*) with 30 pct of unmilled 5083 Al in a transverse section and (*c*) and (*d*) with 50 pct of unmilled 5083 Al in a longitudinal section; (*e*) to (*h*) histograms of grain sizes of the as-extruded 5083 Al alloys.

fractions, loaded in the longitudinal direction. Extensive flow is observed in all the bimodal 5083 Al alloys compressed in the longitudinal direction and inspection of the curves reveals that the strength decreases with increasing volume fraction. The transverse strength also decreases with increasing volume fractions of unmilled powder, as shown in Figure 2(b), albeit

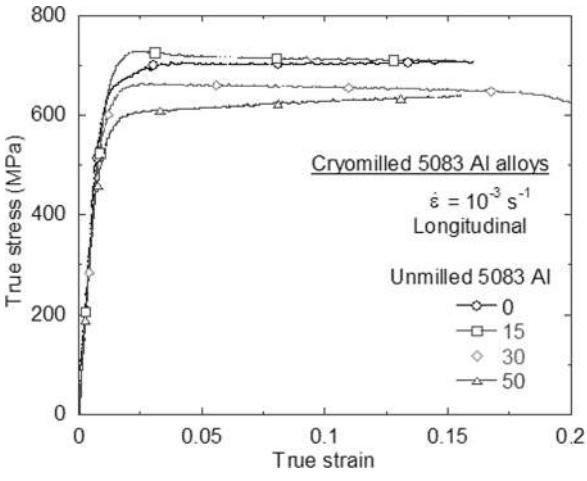

(*a*)

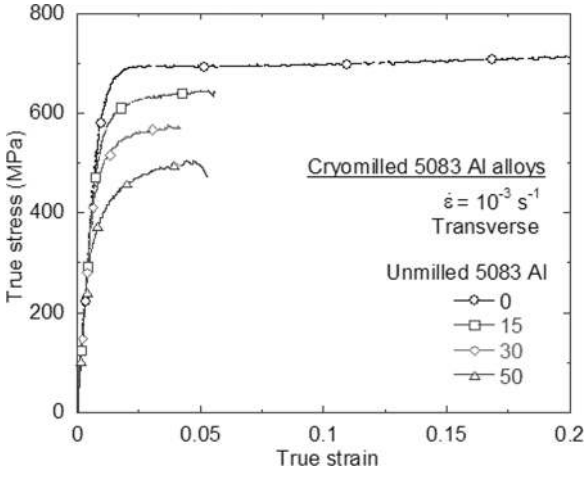

(*b*)

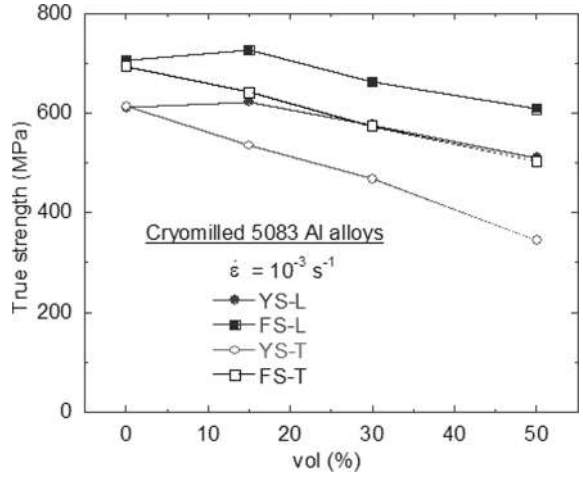

(*c*)

Fig. 2—The effect of volume fraction of unmilled 5083 Al alloys on compressive behavior of bimodal 5083 Al alloys, in the (*a*) longitudinal and (*b*) transverse directions. (*c*) The effect of volume fraction of unmilled 5083 Al alloys on compressive yield strength and flow stress of bimodal 5083 Al alloys in the longitudinal and transverse directions.

more rapidly. The extended compressive deformation in the longitudinal direction is essentially uniform, as evidenced by the morphology of postdeformed compression samples. However, the plastic deformation of the bimodal materials in the transverse direction is brief, and there is a shear failure with an angle of 45 deg to the loading direction after reaching the maximum stress at a strain of only 0.034 to 0.047.

The effect of coarse-grained volume fraction on the compressive yield strength and flow stress at a plastic strain of 0.02 of the as-extruded alloys is shown in Figure 2(c). In the longitudinal direction, there is a negligible difference in both yield strength and flow stress between 0 and 15 pct coarse-grained 5083 Al alloys. However, there is a linear decrease in both yield strength and flow stress from 15 to 30 pct to 50 pct unmilled 5083 Al alloys. In the transverse direction, both yield strength and flow stress decrease linearly with the volume fraction of coarse grains.

C. *Tensile Test*

The tensile behavior of the as-extruded bimodal alloys is shown in Figure 3. The cryomilled 5083 Al alloy with 0 pct coarse-grained fraction showed a high yield strength, followed by a brief work-hardening region, but the specimen failed abruptly without necking. The cryomilled 5083 Al alloys with 15 and 30 pct coarse-grained fraction showed a slightly lower strength and improved ductility, as manifested by the longer work-hardening region and a flow-stress plateau after the ultimate tensile strength. The Young's modulus calculated from the elastic portion of true stress-strain curves is ~69.0 GPa for the cryomilled alloy with 0 pct coarse-grained fraction, 68.8 GPa with 15 pct coarse-grained fraction, and 64.7 GPa with 30 pct coarse-grained fraction, which is similar to the modulus value for pure Al.[13] Obvious necking does not occur, but a Lüders band was observed in the middle of the gage section and final failure occurred at one end of the Lüders band in the bimodal alloys (as shown in Figure 3(b)). The Lüders band appeared to form immediately after the maximum load, and was accompanied by a stress-drop period. During subsequent deformation, intense plastic deformation was localized in the vicinity of the Lüders band.

Figure 3(c) shows the yield strength at an engineering strain of 0.2 pct ($\sigma_{0.2}$), ultimate tensile strength (UTS), uniform strain (ε_u), and elongation-to-failure (ε_f) as a function of coarse-grained volume fraction. Although there is an increase in both ductility and uniform strain for the bimodal 5083 Al alloys with 15 and 30 pct coarse-grained fractions, the volume fraction dependence of both quantities is rather weak. The yield strength and the UTS decreases appear to follow a simple rule of mixtures.

The fracture surfaces of tensile specimens of the as-extruded bimodal alloys were examined using an SEM, as shown in Figure 4. Several distinctive characteristics were noted while examining the sample containing 30 pct coarse grains. First was the existence of a poorly defined dimple morphology in the cryomilled regions, which has been noted in similar cryomilled Al alloys.[11] Second, well-defined dimples were associated with the coarse-grained regions, which are similar to those seen in conventional Al alloys. Necking occurred in the unmilled coarse-grained regions, indicating local ductile failure in these regions. Areas of delamination

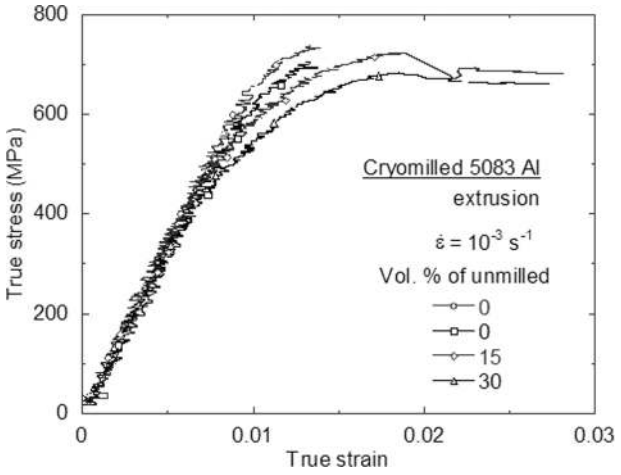

(*a*)

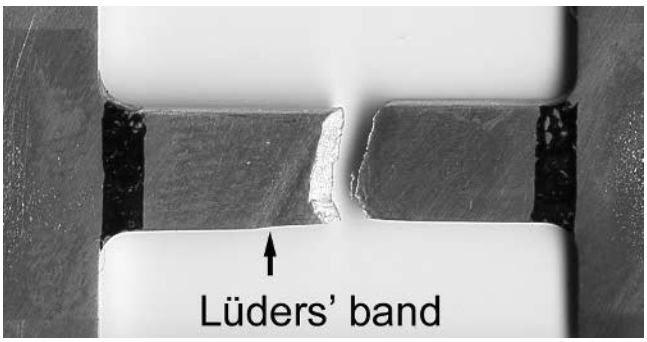

(*b*)

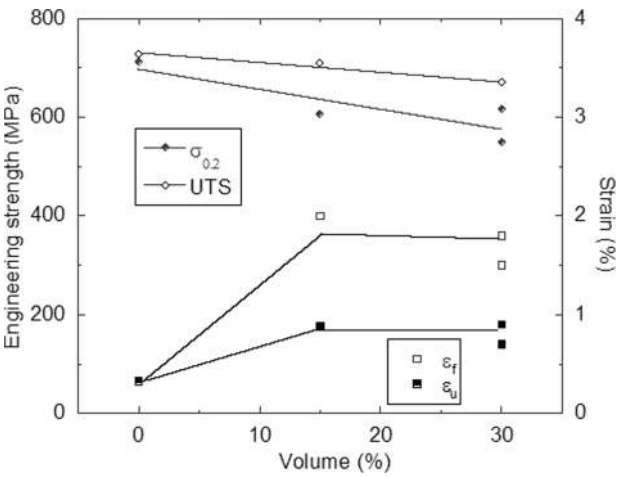

(*c*)

Fig. 3—(*a*) Tensile true strain-stress curves, (*b*) a failed tensile specimen of the as-extruded bimodal 5083 Al alloys with 30 pct coarse grains, and (*c*) volume dependence of engineering strength and strain of the as-extruded bimodal 5083 Al alloys.

were noted at interfaces between the coarse-grained regions and the nanostructured regions. Because no interfacial debonding was observed by TEM in the as-extruded microstructure, the areas of delamination at interfaces must have formed during plastic deformation. Delamination developed around the coarse-grained regions but not uniformly. This suggests that microcracks nucleated on one side of the

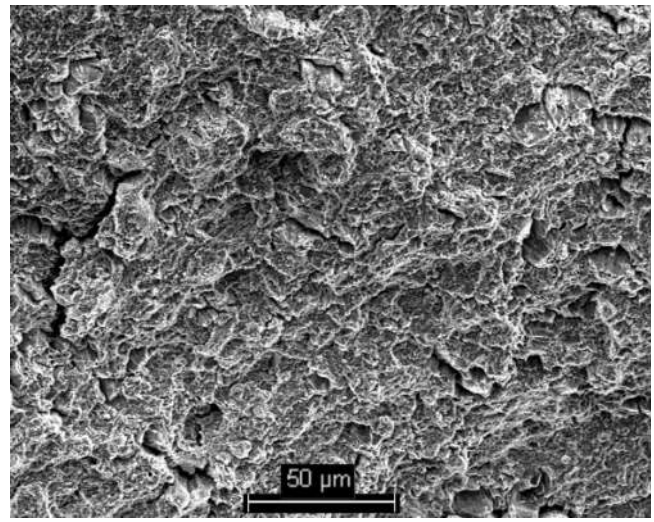

(*a*)

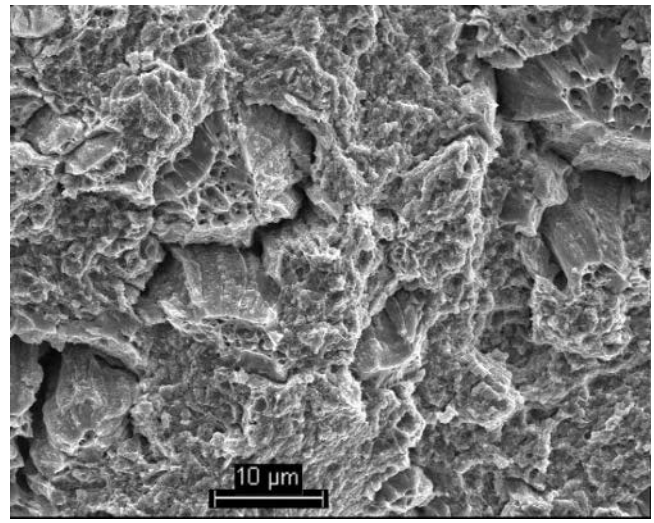

(*b*)

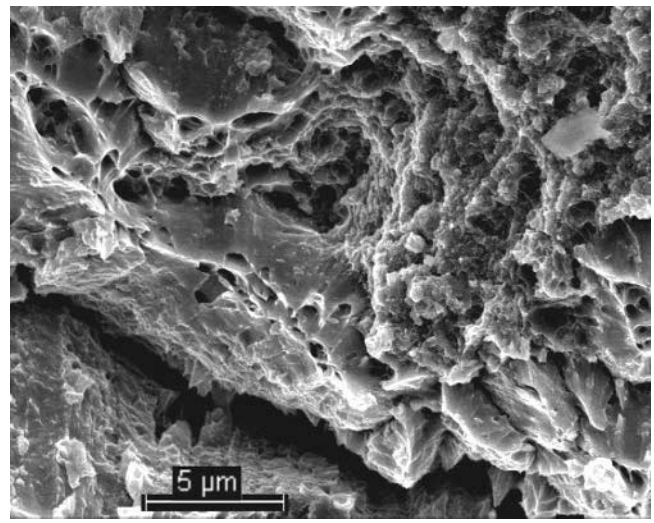

(*c*)

Fig. 4—Fracture surface of the as-extruded 5083 Al alloy containing 30 pct coarse-grained 5083 Al.

coarse-grained regions and propagated to the other (as revealed by Figure 4(b)). In addition, if a microcrack crossed a coarse-grained region from one end rather than from the middle, delamination at interfaces would result in a conical peak without causing failure of the coarse-grained region (as shown in Figure 4(c)).

The tensile behavior of alloy samples in the as-swaged condition was similar to samples in the as-extruded condition. In the present study, the swaging temperature is lower than the extrusion temperature and it is expected that there is a slight improvement of microstructure after swaging or a similar microstructure after the extrusion and the swaging, since both operations are accomplished at rather high temperatures (0.88 T_m *vs* 0.77 T_m). Figure 5(a) shows the true stress-strain response of samples with different coarse-grained volume fractions, while Figure 5(b) summarizes the effect of coarse-grained volume fraction on engineering strength and ductility of the as-swaged cryomilled 5083 Al alloys. For the materials with low additions (15 or 30 pct) of unmilled powder, the strength decrease and ductility increase were approximately linear. However, addition of 50 pct unmilled powder caused a nonlinear strength decrease and ductility increase. As expected, the as-swaged alloy processed from cryomilled powders with 0 pct coarse-grained fraction exhibited a mechanical behavior similar to that of the as-extruded alloy. After the UTS was achieved, a brief stress drop occurred, followed by abrupt failure. For the as-swaged alloy with 15 pct coarse-grained fraction, the yield strength was slightly reduced to 684 MPa. The as-swaged alloy with 30 pct coarse-grained fraction exhibited a linear decrease in yield strength and ultimate tensile strength, and a linear increase in elongation. The alloy containing 50 pct unmilled powder showed a significant decrease in strength, accompanied by a marked increase in elongation. Nevertheless, there was no significant change in the uniform strain (Figure 5(b)). The uniform strain had a weak linear dependence on the volume fraction of unmilled powders. The significant increase in ductility of the 50 pct coarse-grained alloy was attributed to the extended saturated flow stress after reaching the UTS.

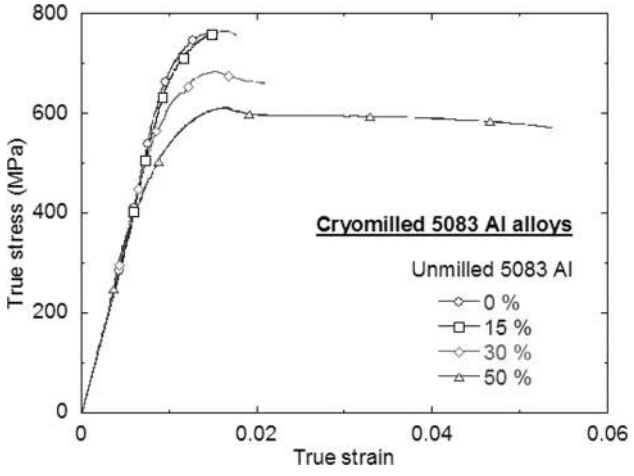

(*a*)

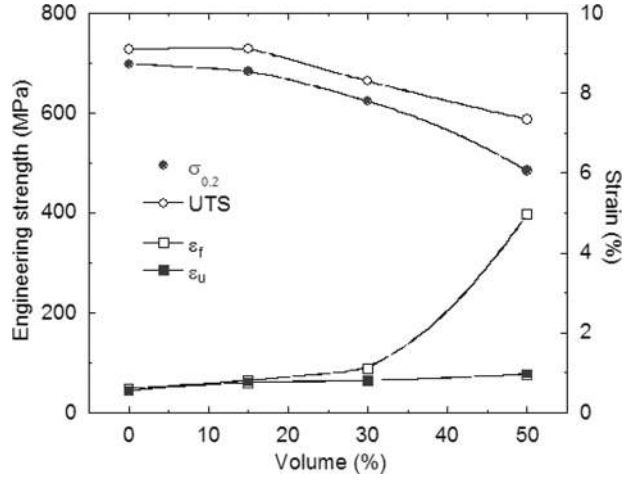

(*b*)

Fig. 5—(*a*) Tensile true strain-stress curves and (*b*) volume fraction dependence of engineering strength and ductility of as-swaged bimodal 5083 Al alloys.

IV. DISCUSSION

A. *Compressive Behavior*

The decrease in compressive strength with increasing coarse-grained volume fraction is expected because the coarse-grained material was softer than the nanostructured regions. However, an unusual aspect of the response was the elastic-perfectly plastic behavior, as evidenced by the relatively flat stress plateaus after yielding. This observation is consistent with findings in other cryomilled nanostructured Al alloys[11,14–16] and results from other nanostructured or ultrafine-grained materials.[17,18,19] This behavior is observed in various fine-grained materials and is attributed primarily to the fine-grained microstructure, as opposed to other metallurgical factors, such as the stacking fault energy.

There are several possible reasons for the apparent absence of significant work hardening during compressive deformation. One possibility is the occurrence of dynamic recovery during plastic deformation. The activation energy for dynamic recovery is expected to be reduced by the presence of residual stress around nanosized dispersoids[11,14–16,20] and an abundance of structural defects present in the alloys. These structural defects might also absorb dislocations generated during plastic deformation. Consequently, the extent of work hardening is limited by the dislocation annihilation and suppression of dislocation accumulation by dynamic recovery. A contributing factor may be that an insufficient number of mobile dislocations during plastic deformation leads to shear localization and shear banding.[17,18,19] Work in this area is continuing.

The compressive strength and ductility in the longitudinal direction of the bimodal 5083 Al alloys are superior to those in the transverse direction. Anisotropy is observed in all the bimodal alloys, as evidenced by the ratio of σ_T/σ_L, which increases with increasing volume fraction of coarse grains. Anisotropy of this kind is not observed in the 100 pct cryomilled sample. In addition, the compressive strain to failure in the transverse direction is less than that in the longitudinal direction, and specimens fail abruptly after a brief period of work hardening. The extrusion processing elongates both nanostructured and coarse-grained regions, leading to the structural defects at interfaces distributed along

the extrusion direction, resulting in mechanical fibering, which has a negative effect on transverse mechanical properties.[15,21] For compressive deformation in the transverse direction, microcracks will form relatively easily at ends of the elongated coarse-grained regions without consuming much energy, resulting in a rapid shear failure.

B. *Tensile Behavior*

The brief period of initial work hardening in the cryomilled 5083 Al alloys resembles behavior observed previously in similar Al-Mg alloys and pure Al.[22,23] In these earlier studies, the behavior was attributed to multiplication of dislocations. Dislocation activity is expected to be restricted in cryomilled Al alloys given the complex microstructure, which includes supersaturated Mg solute, segregation of solute and impurities to grain boundaries, and the possible existence of nanoscale oxide/nitride dispersoids in the matrix.[8,11,24] However, dislocation multiplication over short distances might be possible under sufficiently high applied stresses (well above the yield stress for conventional aluminum). The grain size is approximately 200 nm, which exceeds the critical grain size of several tens of nanometers considered a minimum for the viability of the dislocation activity.[25] When leading dislocations start to move and propagate plastic deformation into adjacent grains, the density of dislocations in the nanostructured region increases, causing work hardening.

The alloys in the present study were designed to have a hybrid microstructure consisting of relatively hard and soft regions. With the addition of a small fraction of unmilled coarse-grained powder to the cryomilled 5083 Al alloy, the majority of the resulting coarse grains are dispersed discretely within the cryomilled nanostructured matrix. The coarse-grained regions are much softer than the nanocrystalline regions. Microhardness measurements performed on the two discrete regions indicated that the nanocrystalline region was approximately 50 pct harder than the coarse-grained regions.[26]

During tensile tests, dislocations build up in both nanostructured and coarse-grained regions. Because of the larger grain size and fewer obstacles to slip, dislocations glide more easily in the coarse-grained regions than in the nanostructured regions. In terms of load transfer, the nanocrystalline regions sustain most of the applied stress and only a small part of the load is transferred to the softer coarse-grained regions. This produces a slight decrease in yield strength. In addition, stress concentrations in the nanostructured regions may be relaxed by transferring local loads to the softer coarse-grained regions, causing flow in the softer coarse-grained regions.[9] These coarse-grained regions are more compliant, not only because of the larger grain size, but also because they lack the impurities (nitrogen, oxygen, carbon, iron, *etc.*) normally associated with cryomilled powders.[8,27] The absence of impurities is likely to facilitate glide in the coarse-grained regions, leading to increased flow during tensile tests.

As the volume fraction of coarse-grained regions is increased, the extrusion-induced flow leads to more contact between coarse-grained regions and, in some cases, coalescence of adjacent particles. The coarse-grained regions become semicontinuous and interpenetrating, resembling the nanostructured regions in distribution and morphology (Figure 1(c)). Consequently, in the 50-50 blended material, both coarse-grained and nanocrystalline regions carry the applied loads. It is noted that although there is an insignificant asymmetry of yield strength between tension and compression of the extruded 5083 Al alloys along the extrusion direction, the plastic deformation behavior in tension and compression is significantly different.

The work-hardening region after yielding is brief in the cryomilled 5083 Al sample with 0 pct coarse-grained fraction but increases in the bimodal alloys. Although the uniform deformation has a weak dependence on the volume fraction of coarse grains (as revealed in Figures 3 and 5), the work-hardening exponent in the work-hardening region decreases with increasing coarse-grained volume fraction. The decreased work-hardening exponent may reduce damage tolerance by limiting the volume of stress concentration ahead of a crack. After the maximum stress is reached, the stress typically drops, and the work-hardening rate diminishes. The slight drop in stress suggests a plastic instability, associated with the formation of necking or cavities.

A similar stress drop phenomenon has been reported in other mechanically alloyed (MA) fine-grained Al alloys[11,28–30] and conventional Al-Mg alloys.[31,32] For example, in an as-extruded MA Al-4Mg-1.5O-0.8C alloy,[28] characterized by a complex network of fine dislocation cells, the stress drop was attributed to the collective movement of large numbers of mobile dislocations that were previously pinned. The subsequent flow stress plateau was attributed to the reduced resistance to glide of unpinned dislocations.

After Lüders band formation, subsequent plastic deformation is observed to accelerate on one side of the Lüders band. In addition, propagation of the Lüders band is limited by the presence of glide obstacles and does not extend across the gage section of the bimodal alloys, although the duration of postyield flow increases with increasing volume fraction of coarse grains. Therefore, the deformation strain after peak stress is mainly related to the formation and propagation of Lüders strain. In summary, the enhancement of ductility in bimodal cryomilled 5083 Al alloys is attributed to two parts, which consist of the increased uniform deformation and the occurrence of Lüders strain.

C. *Enhanced Tensile Ductility*

The concept of ductile-phase toughening of otherwise brittle materials is well established, and variations include inclusions of ductile particles, fibers, or layers.[33–38] By shielding crack tips from applied stress, higher levels of remote stresses can be applied to a ductile-brittle composite material before fracture-critical conditions are reached. Fiber-reinforced composites generally promote greater levels of toughening than particulate-reinforced composites, and ductile-layer reinforced laminates lead to the greatest enhancement of toughening.[38]

The microstructure of the present bimodal alloys is analogous to short-fiber metal matrix composites, in that the coarse-grained bands are distributed parallel to the extrusion direction. The bands tend to be discontinuous when the volume fraction of coarse gains is low, and continuous when the volume fraction of coarse gains is high. However, because the composition of the constituents is nearly identical, there is no mismatch in thermal expansion coefficient or modulus between the two regions in the bimodal cryomilled Al alloys. Consequently, the strength difference between two regions

arises mainly from the differences in grain size and Orowan strengthening.

Several toughening mechanisms have been proposed to explain ductile-phase toughening of composite microstructures, such as crack bridging, crack blunting, crack deflection, stress distribution of crack tip, crack front convolution, and local plane stress deformation.[37,39] For crack bridging to occur, the bridging ligaments must have sufficient ductility to resist fracture at or ahead of the advanced crack tip. Bridging ligaments will restrict crack openings and undergo plastic stretching, thus promoting shielding of the crack tip. An interesting aspect of the process is the constraint of the ductile bands within the harder constituent, which may have implications for the kinetics of the multistep crack growth process.

On the basis of microstructural characteristics observed in the present study, a model of crack blunting combined with the concept of delamination has been developed, as illustrated in Figure 6. The figure shows the propagation of a microcrack in a nanostructured material with a bimodal lamellar structure. In the bimodal Al alloys, microcracks are expected to nucleate first in the harder nanostructured regions and propagate along grain boundaries. When a microcrack meets a coarse-grained band, the band will retard propagation by blunting the crack or by delamination of interfaces between coarse-grained and fine-grained regions, as shown in Figure 6(a). When more dislocations are emitted into the coarse grain, a new slip surface may be formed, eventually leading to necking and cavitation within the coarse-grained bands, as shown in Figure 6(b). Finally, dimples on the coarse-grained regions and delamination at interfaces will be generated on fracture surface (as revealed in Figure 6(c)). If delamination occurs near one end of a coarse-grained band, the final failure of the band will not produce dimples. The delamination at interfaces and the necking deformation of ductile coarse-grained regions will cause significant energy loss, resulting in an enhanced tensile ductility.

A previous theoretical analysis[40] of the effect of interfacial decohesion of metal (ductile phase) in glass (brittle matrix) over a limited length on the force-displacement curve showed behavior analogous to the present experimental analysis. In the case of a crack in glass bridged by a metal fiber, the deformation of a metal fiber is confined to a solid cylinder of height u and diameter $2r$ in a fully constrained deformation.[40] As the metal cylinder extends, it shrinks inward so that its volume remains constant, as expressed by $\Pi \cdot a_o^2 \cdot u_0 = \Pi \cdot r^2 \cdot u$, where u_0 is the initial crack opening and $2a_o$ is the original fiber diameter. In addition, the inward radial displacement δv of any point lying at a radius r results from an axial extension δu, giving an expression $\delta v(r) = -(r/(2u))\delta u$. There are two contributions to the plastic work done on the cylinder: that associated with extending the cylinder and that caused by shrinkage relative to the rest of the fiber

$$\sigma \Pi a_o^2 \delta u = \Pi r^2 \sigma_y \delta u + 2\int_o^r \sigma_s \, 2\Pi r \delta v(r) dr \qquad [1]$$

where σ_s is the shear flow strength of the fiber. Substituting for $\delta v(r)$ and replacing σ_s with $\sigma_y/2$, integration then gives

$$\frac{\sigma}{\sigma_y} = \frac{u_0}{u}\left[1 - \frac{1}{3}\left[\frac{u_0}{u}\right]^{1/2}\frac{a_o}{u}\right] \qquad [2]$$

For the case of limited decohesion at interfaces with a length of l_d (similar to the case of delamination and necking in experiments), the initial crack opening u_0 has to be replaced by the effective decohesion length ($l_d + u_0$). In addition, σ_y increases with strain in the ductile metal cylinder ($\sigma_y = \sigma_0(\varepsilon_y/\varepsilon_o)^n$, where n is the work-hardening exponent, ε_o is the yield strain, and σ_0 is the initial flow stress at yield strain), and the strain in the cylinder can be approximated by ($u/u_0 - 1$). The stress (σ) as a function of displacement (u) of a metal fiber becomes[40]

$$\frac{\sigma}{\sigma_o} = \left[\frac{1}{\varepsilon_o}\left[\frac{u - u_0}{l_d + u_0}\right]\right]^n \left[\frac{l_d + u_0}{l_d + u}\right]\left[1 - \frac{1}{3}\left[\frac{l_d + u_0}{l_d + u}\right]^{1/2}\left[\frac{a_o}{l_d + u}\right]\right] \qquad [3]$$

At a small decohesion length, the force-displacement curve has a peak height, followed by a continuous drop of stress.[40] As the decohesion length increases, the peak in the curve falls, but the curve broadens. When the decohesion length equals the diameter of the ductile fiber, a nearly elastic-perfectly plastic behavior is predicted, much like the behavior observed for the bimodal alloys in the present experimental study. For $n = 0.25$, $\varepsilon_o = 0.004$, and $u_0/a_o = 0.05$, the effect of decohesion on the stress-displacement curve is plotted in Figure 7 for l_o/a_o from 1 to 4. Inspection of the figure reveals that elastic-perfectly plastic behavior is observed when the decohesion length (l_o) is 1 to 2 times larger than the fiber

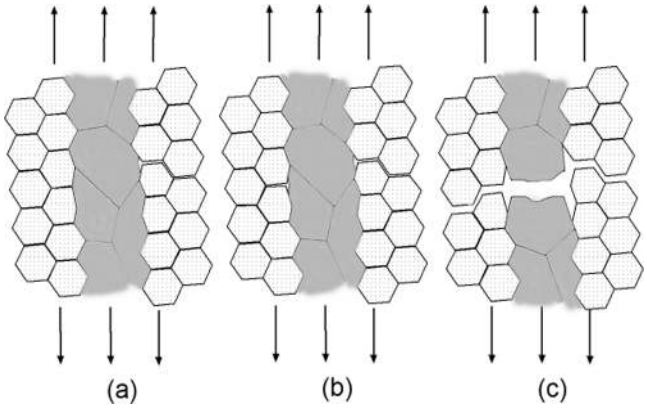

Fig. 6—Crack propagation in the bimodal microstructure.

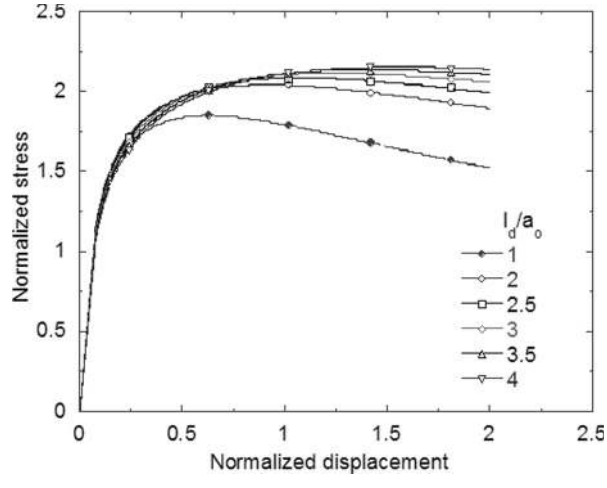

Fig. 7—The effect of decohesion length on the stress-displacement curve.

diameter ($2a_o$). While typical aspect ratios of coarse grain regions in the bimodal alloys were somewhat larger than 1 to 2 (typically 2 to 5 when observed in optical micrographs), the general trends predicted by the theoretical analysis are consistent with the observations of the present study.

V. CONCLUSIONS

Cryomilled 5083 Al alloys were produced by consolidation of blended mixtures of cryomilled and unmilled powders. Microstructural characteristics and mechanical properties were investigated to assess the possible combinations of strength and ductility. A bimodal grain size was achieved in the as-extruded cryomilled 5083 Al alloys with a grain size of 200 nm in nanostructured regions and 1 μm in coarse-grained regions. Elastic-perfectly plastic behavior was observed under compressive loads applied in the longitudinal direction. Anisotropy of compressive behavior was noted, in that strength and ductility were lower in the transverse direction. The anisotropic behavior was attributed to the distribution of elongated coarse-grained regions. In tension, a yield strength of 700 MPa was obtained in the fully cryomilled 5083 Al alloy, which compares favorably with the yield strength of conventional 5083 (145 MPa). As the volume fraction of coarse grains was increased, strength decreased slightly, but ductility increased. An enhanced tensile elongation associated with the occurrence of a Lüders band was observed in bimodal cryomilled 5083 Al alloys. Enhanced tensile ductility was attributed to the occurrence of crack bridging as well as delamination during the plastic deformation.

The results of the present study indicate a process route for the design of microstructures with selected distributions of grain sizes. By combining milled, unmilled, or partially milled powders in select proportions, one can in principle combine constituents of different hardness without the compositional differences normally associated with composite approaches. The powder metallurgy approach demonstrated here relies on the grain size stability afforded by impurities that are incorporated into the powders during cryomilling. When the hardening achieved by grain refinement is coupled with the ductility afforded by incorporation of coarser grains, one can achieve combinations of strength, ductility, and toughness that were previously not possible. A challenge for future work will involve identifying microstructures and process parameters to optimize alloy performance.

ACKNOWLEDGMENTS

Support from the Office of Naval Research (Grant Nos. N00014-03-1-0149 and N00014-03-C-0163) is gratefully acknowledged.

REFERENCES

1. C.C. Koch, D.G. Morris, K. Lu, and A. Inoue: *MRS Bull.*, 1999, Feb., pp. 54-58.
2. X. Zhang, H. Wang, R.O. Scattergood, J. Narayan, C.C. Koch, A.V. Sergueeva, and A.K. Mukherjee: *Appl. Phys. Lett.*, 2002, vol. 81, pp. 823-25.
3. A.A. Karimpoor, U. Erb, K.T. Aust, and G. Palumbo: *Scripta Mater.*, 2003, vol. 49, pp. 651-56.
4. R.Z. Valiev, I.V. Alexandrov, Y.T. Zhu, and T.C. Lowe: *J. Mater. Res.*, 2002, vol. 17, pp. 5-8.
5. K.M. Youssef, R.O. Scattergood, K.L. Murty, and C.C. Koch: *Appl. Phys. Lett.*, 2004, vol. 85, pp. 929-31.
6. Y. Wang, M. Chen, F. Zhou, and E. Ma: *Nature*, 2002, vol. 419, pp. 912-15.
7. G. He, J. Eckert, W. Loser, and L. Schultz: *Nature Mater.*, 2002, vol. 2, pp. 33-37.
8. V.L. Tellkamp, A. Melmed, and E.J. Lavernia: *Metall. Mater. Trans. A*, 2001, vol. 32A, pp. 2335-43.
9. Z. Lee, R. Rodriguez, R.W. Hayes, E.J. Lavernia, and S.R. Nutt: *Metall. Mater. Trans. A*, 2003, vol. 34A, pp. 1473-81.
10. B.Q. Han, F.A. Mohamed, and E.J. Lavernia: *J. Mater. Sci.*, 2003, vol. 38, pp. 3319-24.
11. B.Q. Han, Z. Lee, S.R. Nutt, E.J. Lavernia, and F.A. Mohamed: *Metall. Mater. Trans. A*, 2003, vol. 34A, pp. 603-13.
12. D. Witkin, Z. Lee, R. Rodriguez, S. Nutt, and E. Lavernia: *Scripta Mater.*, 2003, vol. 49, pp. 297-302.
13. H.J. Frost and M.F. Ashby: *Deformation-Mechanism Maps: The Plasticity and Creep of Metals and Ceramics*, Pergamon Press, Elmsford, NY, 1982.
14. S.L. Semiatin, K.V. Jata, M.D. Uchic, P.B. Berbon, D.E. Matejezyk, and C.C. Bampton: *Scripta Mater.*, 2001, vol. 44, pp. 395-400.
15. B.Q. Han, E.J. Lavernia, and F.A. Mohamed: *Mater. Sci. Eng.*, 2003, vol. A358, pp. 318-23.
16. B.S. Dehiya and J.R. Weertman: in *Creep and Fracture of Engineering Materials and Structures*, J.C. Earthman and F.A. Mohamed, eds., TMS, Warrendale, PA, 1997, pp. 129-37.
17. M. Jain and T. Christman: *Acta Metall.*, 1994, vol. 42, pp. 1901-11.
18. J.E. Carsley, A. Fisher, W.W. Milligan, and E.C. Aifantis: *Metall. Mater. Trans. A*, 1998, vol. 29A, pp. 2261-71.
19. D. Jia, K.T. Ramesh, and E. Ma: *Acta Mater.*, 2003, vol. 51, pp. 3495-3509.
20. O. Susegg, E. Hellum, A. Olsen, and M.J. Luton: *Phil. Mag. A*, 1993, vol. 68, pp. 367-80.
21. G.E. Dieter: *Mechanical Metallurgy*, McGraw-Hill, New York, NY, 1986.
22. M. Verdier, Y. Brechet, and P. Guyot: *Acta Mater.*, 1999, vol. 47, pp. 127-34.
23. D. Kuhlmann-Wilsdorf: *Phil. Mag. A*, 1999, vol. 79, pp. 955-1008.
24. F. Zhou, X.Z. Liao, Y.T. Zhu, S. Dallek, and E.J. Lavernia: *Acta Mater.*, 2003, vol. 51, pp. 2777-91.
25. T.G. Nieh and J. Wadsworth: *Scripta Metall. Mater.*, 1991, vol. 25, pp. 955-58.
26. Z. Lee, D.B. Witkin, E.J. Lavernia, and S.R. Nutt: *MRS Proc.*, Materials Research Society, Pittsburgh, PA, 2003, vol. 740, pp. I1.7.1-I1.7.6.
27. F. Zhou, J. Lee, S. Dallek, and E.J. Lavernia: *J. Mater. Res.*, 2001, vol. 16, pp. 3451-58.
28. Y.W. Kim and L.R. Bidwell: *Scripta Metall.*, 1982, vol. 16, pp. 799-802.
29. T. Mukai, K. Ishikawa, and K. Higashi: *Mater. Sci. Eng.*, 1995, vol. A204, pp. 12-18.
30. H.R. Last and R.K. Garrett: *Metall. Mater. Trans. A*, 1996, vol. 27A, pp. 737-45.
31. D.J. Lloyd: *Met. Sci.*, 1980, May, pp. 193-98.
32. D.J. Lloyd: *Metall. Trans. A*, 1980, vol. 11A, pp. 1287-94.
33. L.S. Sigl, P.A. Mataga, B.J. Dalgleish, R.M. McMeeking, and A.G. Evans: *Acta Metall.*, 1988, vol. 36, pp. 945-53.
34. P.A. Mataga: *Acta Metall.*, 1989, vol. 37, pp. 3349-59.
35. M. Bannister, H. Shercliff, G. Bao, F. Zok, and M.F. Ashby: *Acta Metall.*, 1992, vol. 40, pp. 1531-37.
36. M. Hoffman, B. Fiedler, T. Emmel, H. Prielipp, N. Claussen, D. Gross, and J. Rodel: *Acta Metall.*, 1997, vol. 45, pp. 3609-23.
37. D.R. Lesuer, C.K. Syn, O.D. Sherby, J. Wadsworth, J.J. Lewandowski, and J.W.H. Hunt: *Int. Mater. Rev.*, 1996, vol. 41, pp. 169-97.
38. A.B. Pandey, B.S. Majumdar, and D.B. Miracle: *Acta Mater.*, 2001, vol. 49, pp. 405-17.
39. W. Soboyejo: *Mechanical Properties of Engineered Materials*, Marcel Dekker, Inc., New York, NY, 2003.
40. M.F. Ashby, F.J. Blunt, and M. Bannister: *Acta Metall.*, 1989, vol. 37, pp. 1847-57.